

# Magnetic Field Homogeneity Adjustment for Magnetic Resonance Imaging Equipment

I. Frollo<sup>1</sup>, P. Andris, A. Krafčík, D. Gogola, and T. Dermek

Institute of Measurement Science, Slovak Academy of Sciences, 841 04 Bratislava, Slovakia

Imaging based on magnetic resonance (MR) methods needs a source of the highest homogeneous magnetic field in the whole volume of the investigated object. The goal of this paper is to demonstrate three methods of correcting coils (shim coils) current calculations and homogeneity adjustment on a whole-body MR imager, based on three methods for static magnetic field measurements. Measurements are carried out using: magnetometer based on the Hall effect, nuclear MR point magnetometer, and gradient-echo imaging method applied to circular test tubes. All three measurements measure the magnetic field on a circle (12 measuring points) and one point in the center. A set of linear equations, determination of a target function, and optimization computations are procedures that provide optimal values of currents for correcting coils. Results of all three methods are compared and discussed. The proposed methods are suitable for periodic testing and correction of magnet inhomogeneities for MRI magnets.

**Index Terms**—Magnetic field homogeneity calculation, magnetic field measurement, nuclear magnetic resonance (NMR) imaging.

## I. INTRODUCTION

MEASUREMENT and imaging methods based on magnetic resonance (MR) principles need a static homogeneous magnetic field with highest homogeneity in the whole measurement object volume [1]–[3]. No constructed magnet (permanent or electromagnet) generates a perfect homogeneous magnetic field, and therefore, an ingenious coil system construction fed by separate current power supplies for compensation (shimming) of particular magnetic inhomogeneous components ( $x$ ,  $y$ ,  $xy$ ,  $yz$ ,  $xz$ ,  $x^2 - y^2$ ,  $xz^2$ ,  $yz^2$ ,  $z$ ,  $z^2$ ,  $z^3$ ,  $z^4$ , ...) is needed (Fig. 1).

A comprehensive measurement method and mathematical computation for individual shim current setting are needed, for commercial imagers manufactured by the magnet producer [4]. Final shim currents are set directly on site after real magnetic field inhomogeneities measurements are performed using nuclear MR (NMR) magnetometers or directly by imaging [5]. Periodical basic magnet homogeneity testing during its operation, especially in situations when ferromagnetic object distribution near the magnet is changed and when the magnet is not equipped with magnetic shielding, is needed.

Numerous methods for magnetic field correction and shim coils current calculation have been developed, generally based on the spherical harmonic expansions and their derivatives. Computation of the coefficients for every component of the expansion using minimization methods was published in [1] and [4]. First attempts to measure the magnetic field of a whole-body imager, using NMR Gaussmeter and the least square method for the homogeneity optimization, was published in [6]. Using a rapid spherical harmonic calculation method, it is possible to correct the magnetic field to achieve the highest homogeneity [7], [11]. Passive shim design and

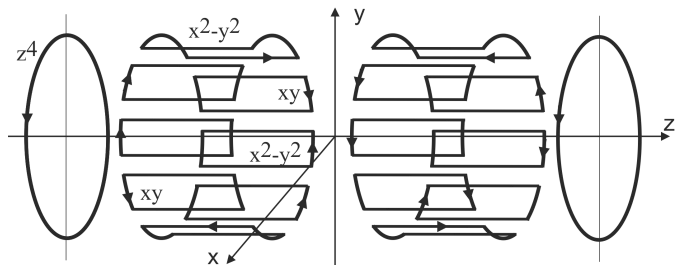


Fig. 1. Image of selected shimming coils of the whole-body MRI imager.

a shimming approach for biplanar permanent MR imaging magnets were published in [13] and [14]. Finite-length MR shim coils and shielded zonal and tesseral coils were designed by Forbes and Crozier [15]–[17]. A method for the design of streamline coil designs is detailed and patterns for third-order ellipsoidal shims wound on a cylindrical surface are presented in [18]. A method for calculating the currents and winding patterns required to design independent zonal and tesseral shim coils for MR imaging is presented in [19]. An efficient design method of axial shim coils for MRI is presented in [20]. In this paper, the axial shim coils are designed to improve magnetic field homogeneity which compensates for the unavoidable construction tolerances, cold shrink of magnet frame, and some other negative effects. A novel nonlinear optimization algorithm for designing a shim coil system, especially a high-order axial shim coil, for MR imaging was presented in [21]. A gradient shimming based on the regularized estimation for B-0-field and shim functions is published in [22]. Based on a statistical model, the B-0-field and shim function maps are estimated by a penalized maximum likelihood method that minimizes two regularized least-squares cost functions. A numerical method with an inverse boundary element method to design a set of shim coils for an open biplanar superconducting MR imaging system is proposed in [23]. A shimming calculation method, which can calculate iron piece placements rapidly to make the magnetic field homogeneous at intended homogeneity and then

Manuscript received November 6, 2017; revised December 6, 2017, January 15, 2018, and February 2, 2018; accepted February 5, 2018. Date of publication March 2, 2018; date of current version April 17, 2018. Corresponding author: I. Frollo (e-mail: frollo@savba.sk).

Color versions of one or more of the figures in this paper are available online at <http://ieeexplore.ieee.org>.

Digital Object Identifier 10.1109/TMAG.2018.2804352

to make the shimming working time short is proposed in [24]. Routine testing of magnetic field homogeneity on clinical MRI systems (ranging in field strength from 0.2 to 3.0 T) was published in [25]. Fast gradient-echo (GE) pulse sequences were scanned twice using small and large bandwidth difference.

Interesting results were published in the next three papers—MR imaging in the magnetic field without using shim coils. The calculated polynomial coefficients composing the  $zy$ -plane (2-D imaging plane) of the Halbach spatial encoding field are published in [26]. Using an inhomogeneous small-scale magnet for spatial encoding in lieu of gradient coils, a lightweight scanner for 2-D MR imaging was constructed. A simple method for measurement and correction of off-resonance related geometric distortion in echo-planar imaging (EPI) was published in [27]. This method is robust for unwarping EPI images of the human brain, and it is currently a routine step in the processing of EPI image sets for functional brain activation studies. Robust field map generation using a triple-echo acquisition [28] was used for generating magnetic field maps for the correction of geometric distortions in echo-planar MR images. The method is feasible in every fMRI scanning session, calculate field maps, and correct geometric distortions of the functional images as a routine procedure.

In this paper, we are describing a new, simple and as to the measurement and calculation fast method for shim coil current computation based on magnetic field values measured without shim coils (currents for shim coils are switched OFF) and magnetic field values after switching on the shim coils testing currents.

## II. THEORY OF SHIMS

Compliance with the conditions of homogeneity of the magnetic field enables realization of the measuring process for this device. For the purposes of MR-tomography is the size of the required inhomogeneity on the order of  $10^{-5}$  in the field of measurement. Inhomogeneity of the magnetic field is determined by

$$\Delta = \max \left[ \frac{|B(x, y, z) - B(0, 0, 0)|}{B(0, 0, 0)} \right] \quad (1)$$

where  $B(x, y, z)$  is the size of the magnetic induction in the point  $(x, y, z)$  and  $B(0, 0, 0)$  indicates the size of the magnetic induction at the beginning of the coordinate system.

From the stringent requirements placed on the accuracy of this configuration of the magnetic field follow requirements on the source of the magnetic field in terms of design, construction, and location. For computed tomography using MR, as the sources of a magnetic field, the following types of magnets are used: resistive, superconducting, and permanent.

In terms of acquisition and operational costs and in terms of the location, the resistive magnets are the best magnets in many cases of clinical use. They are made up of a set of coils mirrored symmetrically, spaced relative to the center plane ( $z = 0$ ) along the main axis ( $z$ -axis) of the magnet (Fig. 2) and powered by the external current source. In view of the need for access to the sample (the human body) in the field of measurement and given technology of the winding coils production with the required accuracy,

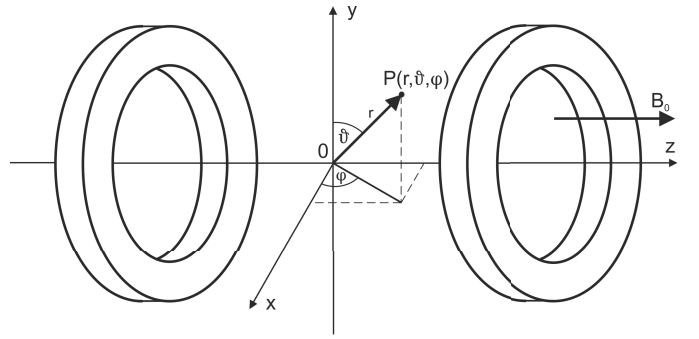


Fig. 2. Rotationally and mirrored symmetrical double coil of the magnet.

the rotational symmetry is preferable. Rotational symmetry with respect to the axis of the magnet at the same time eliminates the dependence of the magnetic field generated from the azimuthal components.

Today, quite well sophisticated methods of synthesis of a magnetic field are known, for example, [8]–[10], allowing a theoretical proposal for the magnets, which are characterized in terms of MR-tomography with sufficient homogeneity. Deviations from the theoretical proposal arising in the construction of magnets most often by non-compliance with calculated dimensions of the winding coils and their positioning carry the considerable errors to the magnets' theoretical design.

The next source of substantive errors of the chosen configuration of the magnetic field is the environment, in which the magnet, as part of MR-tomography, is placed. A summary of these errors will cause the enlargement of the field inhomogeneity in the area of measurement, reducing the volume of the measuring field of the homogeneity and this will limit or often make measurement impossible on the MR-tomography. It is possible to eliminate unwanted effect of these errors by correction of the magnetic field in the area of measurement.

The aim of this part is to show the proposal of the optimization analysis process of static magnetic field in a certain area (area of measurements for the purpose of MR-tomography).

### A. Analysis of the Static Magnetic Field

Examination of homogeneity, the precision of the specific configuration of the magnetic field, and its correction would not be completed without an accurate description and analysis of the field. In the measuring field of the MR-tomography, the spatial distribution of magnetic field is determined by vector shape of the Laplace differential equation

$$\Delta \mathbf{B} = 0 \quad (2)$$

where  $\Delta$  is the Laplace operator and  $\mathbf{B}$  is the magnetic field induction vector.

Due to the rotational symmetry of the majority of the magnets for the MR-tomography, Fig. 2, we describe the magnetic field in spherical coordinates. Solution of Laplace equation for each component of the  $\mathbf{B}$  expressed in the form

of the development of spatial spherical functions

$$B_i(r, \vartheta, \varphi) = \sum_{n=0}^{\infty} U_n(r, \vartheta, \varphi) = \sum_{n=0}^{\infty} r^n S_n(\vartheta, \varphi) \\ = \sum_{n=0}^{\infty} r^n \sum_{k=0}^n [A_n^k \cos(k\varphi) + B_n^k \sin(k\varphi)] P_n^k(\cos \vartheta) \quad (3)$$

where

- $U_n(r, \vartheta, \varphi)$  the spatial spherical function of  $n$ th order,  $S_n(\vartheta, \varphi)$ —surface sphere function of  $n$ th order on radius  $r$ ;
- $P_n^k(\cos \vartheta)$  Legendre combined polynomial of the degree of  $n$  and of  $k$ th order;
- $A_n^k$  and  $B_n^k$  factors characterizing the size of members of the degree  $n$  and of the order  $k$  of the expansion. where index  $i$  is characterized by the particular rectangular components of the  $\mathbf{B}$ , and so  $B_x$ ,  $B_y$ , and  $B_z$ .

This shape is due to the development of the orthogonal-ity (3) on the surface of the spherical space, useful for the purposes of the magnetic field correction.

In the magnets for the MR-computed tomography with rotational symmetry of coils is the vector of the magnetic field induction mainly oriented to the direction of the main axis ( $z$ -axis), and the components  $B_x$  and  $B_y$  of the vector  $\mathbf{B}$  could be, due to their size, neglected [1]. Then, for the mag-netic induction in the field of measurements, on the basis of the relationship (3), transferring to the rectangular coordinate system, we can write

$$B_Z(X, Y, Z) \\ = A_0^0 + A_1^0 Z^1 - A_1^1 X^1 - B_1^1 Y^1 - A_2^0 \left( \frac{X^2}{2} + \frac{Y^2}{2} - Z^2 \right) \\ - 3A_2^1 X^1 Z^1 - 3B_2^1 Y^1 Z^1 + 3A_2^2 (X^2 - Y^2) + 6B_2^2 X^1 Y^1 \\ - \frac{3}{2} A_3^0 Z^1 \left( X^2 + Y^2 - \frac{2}{3} Z^2 \right) \\ + \frac{3}{2} A_3^1 X^1 (X^2 + Y^2 - 4Z^2) + \frac{3}{2} B_3^1 Y^1 (X^2 + Y^2 - 4Z^2) \\ + 15A_3^2 Z^1 (X^2 - Y^2) + 30B_3^2 X^1 Y^1 Z^1 \\ + 45A_3^3 X^1 \left( -\frac{1}{3} X^2 + Y^2 \right) - 45B_3^3 Y^1 \left( X^2 - \frac{1}{3} Y^2 \right) \\ + 3A_4^0 \left( \frac{1}{8} X^4 + \frac{1}{8} Y^4 + \frac{1}{3} Z^4 + \frac{1}{4} X^2 Y^2 - X^2 Z^2 - Y^2 Z^2 \right) \\ + \frac{15}{2} A_4^1 X^1 Z^1 \left( X^2 + Y^2 - \frac{4}{3} Z^2 \right) \\ + \frac{15}{2} B_4^1 Y^1 Z^1 \left( X^2 + Y^2 - \frac{4}{3} Z^2 \right) \\ + 15A_4^2 \left( 3X^2 Z^2 - 3Y^2 Z^2 - \frac{1}{2} X^4 - \frac{1}{2} Y^4 \right) \\ - 15B_4^2 X^1 Y^1 (X^2 + Y^2 - 6Z^2) \\ + 315A_4^3 X^1 Z^1 \left( -\frac{1}{3} X^2 + Y^2 \right) - 315B_4^3 Y^1 Z^1 \left( X^2 - \frac{1}{3} Y^2 \right) \\ + 105A_4^4 (X^4 + Y^4 - 6X^2 Y^2)$$

$$+ 420B_4^4 X^1 Y^1 (X^2 - Y^2) + \dots \quad (4)$$

where

- $A_0^0$  size of the magnetic induction in the origin;
- $A_1^0$  change of the magnetic induction along the  $z$ -axis;
- $A_1^1$  and  $B_1^1$  change of the magnetic induction along the  $x$ - or  $y$ -axis;
- $A_2^0$  change of the magnetic induction. It is quadratically increasing along the  $z$ -axis and quadratically decreasing along the  $x$ - or  $y$ -axis, ... etc.

Because of the relationship (3), individual members of development (4), characterized by coefficients  $A_n^k$  or  $B_n^k$ , [ $n, k$ , in the limits according to the relative size according to (3)], are orthogonal values of the magnetic field induction. The coefficient  $A_0^0$  indicates the homogeneous component of the field in the middle of the measurement field, and the remaining members of development (4), determining the size of particular orthogonal field gradients, present the non-homogenous components of the field. For MR-tomography it is an effort to create a homogeneous field in the area of measurement and it is therefore necessary to eliminate unwanted effects of each gradient of the basic magnetic field.

### B. Finding an Approximative Polynomial

The theory of partial differential equations shows that the solution to (2), which determines the spatial distribution of the magnetic field in the area of measurement, is fully determined by the values of the variables (induction of the magnetic field) on the boundary of the measurement area. In MR imaging the measurement area is usually equivalent to the space in the shape of a ball and boundary surface is in this case the surface of the ball. The individual values of the operative parameters on the surface are found by measurement. Development of the functions of the operative parameters of a magnetic field by the relation (3) is possible for every smooth function. In general, the development of (3) has an infinite number of members and only in the case of the function determining variables in the form of a rational function has the whole range of (3) a finite number of elements.

For this special case, the size of each of the coefficients  $A_n^k$  or  $B_n^k$ , formula (3), is calculated according to (5). Other-wise, using the general functions of the development according to the relation (3) to determine the size of particular gradients in the field of measurement, we are forced to restrict in practice the actual infinite series (3) on a finite number of members

$$E(r, \vartheta, \varphi) = \sum_n r^n \sum_{k(n)} [A_n^k \cos(k\varphi) + B_n^k \sin(k\varphi)] P_n^k(\cos \vartheta) \quad (5)$$

while  $\max [k(n)] \leq n$ , where  $E(r, \vartheta, \varphi)$  is a polynomial approximation with finite number of members that are selected from the infinite set of coefficients of the sequence (3). In this way, an error is arising between the actual value of the operative functions and the value established on the basis of the approximation polynomial (5).

To minimize this error on the measurement area, the least-squares method will be used. The sum of the squared differences in particular points of measurement belonging to the bounding area on the surface of the sphere is

$$F(A_n^k, B_n^k) = \sum_m \sum_{l(m)} [f(r, \vartheta_m, \varphi_l) - E(r, \vartheta_m, \varphi_l)]^2 \quad (6)$$

where  $f(r, \vartheta_m, \varphi_l)$  indicates the size of the operative field parameter of the boundary area in the measurement points with the positions defined by values  $r$ ,  $\vartheta_m$ , and  $\varphi_l$  in spherical coordinates.  $F(A_n^k, B_n^k)$  represents the size of the sum of quadrates of differences in the measuring points depending on the values of the coefficients  $A_n^k$  and  $B_n^k$  of the approximative polynomial  $E(r, \vartheta, \varphi)$ .

The finding of the minimum of the function  $F(A_n^k, B_n^k)$  given by (6) is leading, according to the extreme functions definition of more variables, to the system of equations

$$\begin{aligned} & \sum_n \sum_{k(n)} A_n^k \left\{ r^n \sum_m [P_n^k(\cos \vartheta_m) P_n^{k'}(\cos \vartheta_m) \right. \\ & \quad \left. \cdot \sum_{l(m)} \cos(k\varphi_l) \cos(k'\varphi_l)] \right\} \\ & + \sum_n \sum_{k(n)} B_n^k \left\{ r^n \sum_m [P_n^k(\cos \vartheta_m) P_n^{k'}(\cos \vartheta_m) \right. \\ & \quad \left. \cdot \sum_{l(m)} \cos(k\varphi_l) \cos(k'\varphi_l)] \right\} \\ & = \sum_m \sum_{l(m)} f(r, \vartheta_m, \varphi_l) \cos(k'\varphi_l) P_n^{k'}(\cos \vartheta_m), \end{aligned}$$

and

$$\begin{aligned} & \sum_n \sum_{k(n)} A_n^k \left\{ r^n \sum_m [P_n^k(\cos \vartheta_m) P_n^{k'}(\cos \vartheta_m) \right. \\ & \quad \left. \cdot \sum_{l(m)} \cos(k\varphi_l) \sin(k'\varphi_l)] \right\} \\ & + \sum_n \sum_{k(n)} B_n^k \left\{ r^n \sum_m [P_n^k(\cos \vartheta_m) P_n^{k'}(\cos \vartheta_m) \right. \\ & \quad \left. \cdot \sum_{l(m)} \sin(k\varphi_l) \sin(k'\varphi_l)] \right\} \\ & = \sum_m \sum_{l(m)} f(r, \vartheta_m, \varphi_l) \sin(k'\varphi_l) P_n^{k'}(\cos \vartheta_m) \quad (7) \end{aligned}$$

where  $\max[k(n)] \leq n$ , and the indices  $n'$  and  $k'$  acquire the values of the coefficients  $A_n^k$  and  $B_n^k$  of the equation (5). As solution of equations (7), we obtain the values of the coefficients  $A_n^k$  or  $B_n^k$  of (5) for which shall function  $F(A_n^k, B_n^k)$ , determined by the relationship (6), acquire its minimum. On the basis of the relationship (4) are, by the values of these coefficients  $A_n^k$ ,  $B_n^k$ , determined the values of the gradients of the analyzed magnetic field.

To the rest of the gradients of the magnetic field, which are not contained in the approximative polynomial  $E(r, \vartheta, \varphi)$ , we assign a zero size.

The number of members of the approximation polynomial is dependent on the required accuracy of the function  $f(r, \vartheta, \varphi)$  given by the polynomial. Then, on the area (bordering area of measurement) must be performed the inequality

$$|f(r, \vartheta, \varphi) - E(r, \vartheta, \varphi)| \leq \delta \quad (8)$$

where  $\delta$  is the value of the maximal deviation between the actual and approximate value of the magnetic field with respect to determining the quantity of the accuracy of the analyzed area.

By measurements we get the values of the function  $f(r, \vartheta, \varphi)$  of the individual points, and hence, inequality (8) can be assessed only at discrete points in the area. To assess the validity of this relationship to the whole of the area, it would be necessary to know the value of the left side of the inequality (8) over the whole area, which is practically impossible. Therefore, we assess the inequality (8) indirectly, by means of the left part boundary of this expression.

We assume that when assessing the validity of the relationship (8) on the whole of the region, a network of points of measurement of the operative functions of the magnetic field is sufficiently dense, that for each point of measurement to the field is true

$$|f(H_K) - f(H_{KSi})| \leq \Delta f_{\max} \quad (9)$$

where  $i = 1, 2, \dots, n$ ,

$H_K$	any point of setting the measuring points;
$H_{KSi}$	$i$ th value to the point $H_K$ , neighboring point of network points measurement;
$f(H_K)$ and $f(H_{KSi})$	the functional values of the operative function of the magnetic field in points $H_K$ and $H_{KSi}$ ;
$\Delta f_{\max}$	the allowed value of the maximal difference for the values of the determining function in any two adjacent points of measurement.

In search of the approximation polynomials of specific magnetic fields, we set out comparing the sustainability of the determined shape with approximative polynomial, containing the members of the higher order too as a given polynomial.

In the case that the magnetic field encompasses, considering the required accuracy of approximation, the gradients of the not negligible values, characterized by some of these members, the size of these members of the order (5) is significantly larger than the size of the remaining members of the higher degree and order, and comparable or larger than the size of minimal members of the initially approximative polynomial. In this case, we will include into the approximative polynomial these members too, and by the above described procedure we optimize the number of members in the light of the requirement of the minimum of the number and complexity

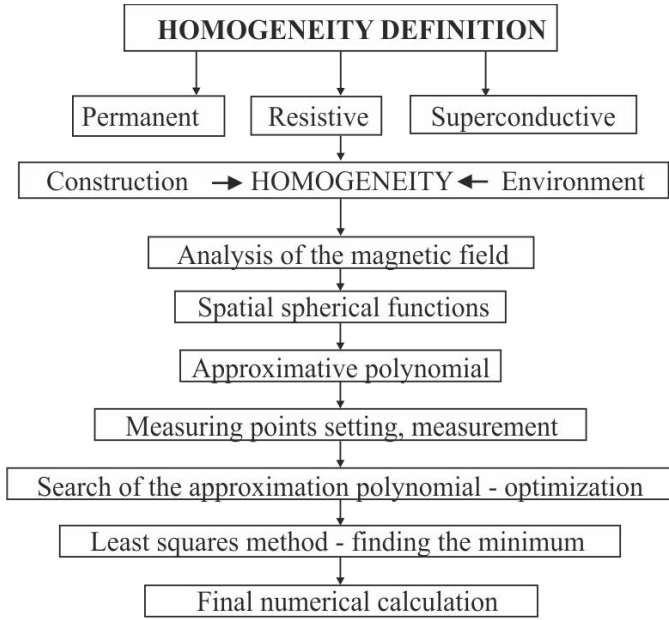


Fig. 3. Short graphical presentation of the above described theory.

of their elimination, which reduces the number of members of an approximative polynomial in comparison with the initial shape of the polynomial.

With regard to the accuracy of the approximation, as described, it is possible to optimize static magnetic field approximation polynomial (the maximum degree of approximation and the selection of the members and capabilities of elimination in the process of the field correction) as well as the option of the location and number of measuring points selection of the physical reality (the static magnetic field).

This section is presented in a relative concise way. For better understanding the theoretical section, a flow chart was added to the text (Fig. 3).

In Section III, we show a simplified, but in terms of measurement and calculation, an effective way of magnetic field parameters analysis and its real corrections.

### III. SUBJECT AND METHODS

For driving currents calculation of  $n$  correction coils it was necessary to measure magnetic flux density of pure original uncorrected basal field  $\mathbf{B}_j^{0,uc}$ , as well as magnetic flux density contribution of each correction coil separately with the same initial driving current, e.g.,  $I_0 = 1$  A, in  $m$  probe points ( $\mathbf{B}_{i,j}^c$ , for  $i \in \{1, \dots, n\}$ ,  $j \in \{1, \dots, m\}$ ).

The proper optimization assumes linear contribution (in driving currents) of each correction coil to the basal field; therefore, the resultant field is a superposition of all correction fields and basal field. This could be mathematically expressed as a system of linear equations

$$\mathbf{B}_j^{0,c} = \mathbf{B}_j^{0,uc} + \sum_{i=1}^n \mathbf{B}_{j,i}^c I_i \quad (10)$$

where  $\mathbf{B}_j^{0,c} = \mathbf{B}_0$ , for  $j \in \{1, \dots, m\}$ , is desired corrected field  $\mathbf{B}_0$  in  $j$ th probe point, and  $I_i$  is the unknown current of  $i$ th

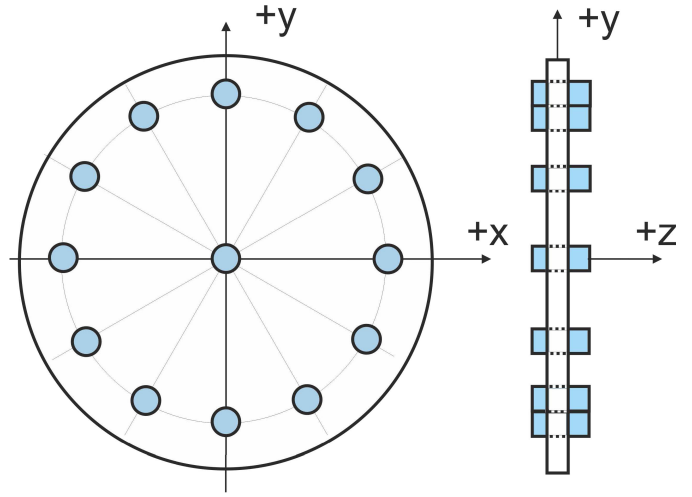


Fig. 4. Circular module equipped with 13 capsules (measuring transducers) placed in a holder in the  $xy$ -plane. Diameter of the capsules circle is 200 mm. Diameter/length of the capsules are 15 mm/55 mm.

correction coil. System of linear equations (10) is soluble by simple linear decomposition. For instance, solution of this system of linear equations can be provided by the backslash operator in MATLAB, i.e.,  $\mathbf{I} = \mathbf{A} \backslash \mathbf{b}$ , where

$$\mathbf{A} = \begin{pmatrix} B_{11x} \dots B_{1nx} \\ \vdots \\ B_{m1x} \dots B_{mnx} \\ B_{11y} \dots B_{1ny} \\ \vdots \\ B_{m1y} \dots B_{mny} \\ B_{11z} \dots B_{1nz} \\ \vdots \\ B_{m1z} \dots B_{mnz} \end{pmatrix}_{3m \times n} \quad \mathbf{b} = \begin{pmatrix} B_{0x} \\ \vdots \\ B_{0x} \\ B_{0y} \\ \vdots \\ B_{0y} \\ B_{0z} \\ \vdots \\ B_{0z} \end{pmatrix}_{3m \times 1} - \begin{pmatrix} B_{10x} \\ \vdots \\ B_{m0x} \\ B_{10y} \\ \vdots \\ B_{m0y} \\ B_{10z} \\ \vdots \\ B_{m0z} \end{pmatrix}_{3m \times 1} \quad (11)$$

and

$$\mathbf{I} = (I_1 \dots I_n)_{1 \times n}^T \quad (12)$$

with definitions:  $B_{jia} = (\mathbf{B}_{j,i}^c)_a$ ,  $B_{0a} = (\mathbf{B}_0)_a$ , and  $B_{j0a} = (\mathbf{B}_j^{0,uc})_a$  for  $a \in \{x, y, z\}$  and for  $m$ -points and  $n$ -coils.

For measurements, a circular disc with 13 measuring holes was constructed (Figs. 4 and 5). The holes served for inserting measuring sensors or capsules with measuring liquid for imaging.

For magnetic field measurements and optimal shim coil current calculation, three methods—instrumentations were used.

In general, measurement was repeated in three positions of the circular module, in the center of the basic magnet and moved  $-100$  mm (left) and  $+100$  mm (right) in the  $z$ -direction.

The calculation procedures were formally performed by the following algorithm:

- 1) Magnetic field measurement in 3 planes, received 3 data files. This is the magnetic field without any corrections in all 39 points.

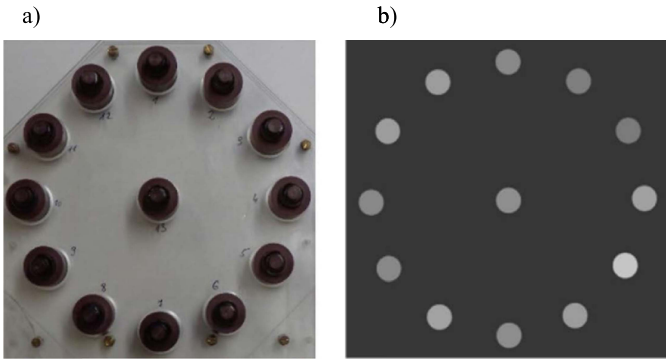


Fig. 5. Measuring capsules placed in a holder in the  $xy$ -plane. (a) Real positioning of measuring transducers. (b) MR image of 13 capsules (average values).

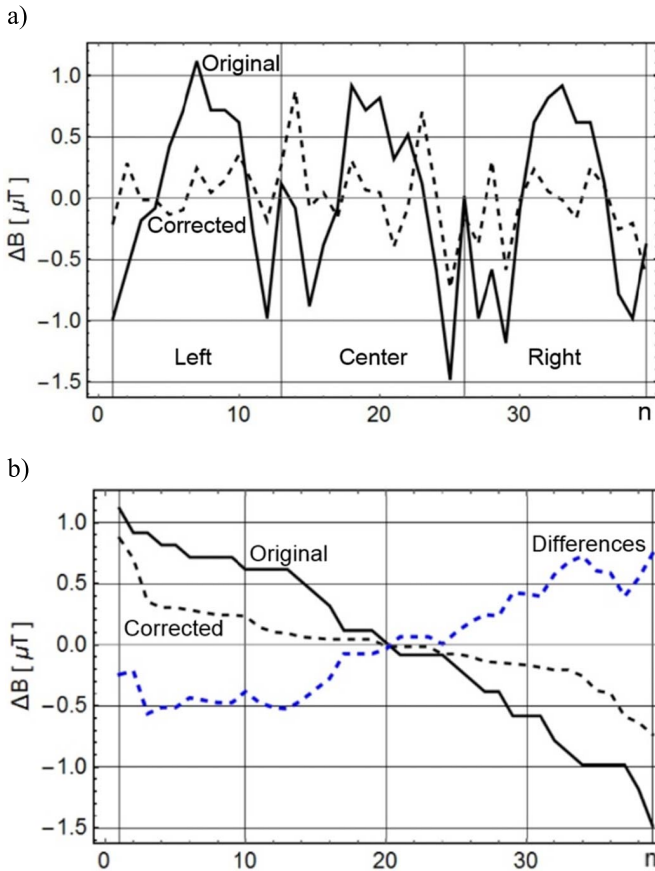


Fig. 6. (a) Graphical display of  $n = 39$  values of the magnetic field contributions (three planes in the  $z$ -direction, left, center, and right), measured by teslameter based on the Hall effect. (b) Values sorted according to size and differences.

- 2) Calculation of the mean values and deviations from the mean value. These are input quantities for the shim coils currents calculation.
- 3) Calculation of inhomogeneity values = max. – min. values.
- 4) Testing of 14 shim coils ( $x, y, xy, yz, xz, x^2-y^2, xz^2, yz^2, z, z^2, z^2s, z^3, z^4, z^4s$ ) magnetic field contributions. Coils are fed by currents 1, 5, or 10 A and resultant magnetic field contributions were recalculated for 1 A. The goal is to find out each shim coil contribution of the magnetic field caused by 1 A.

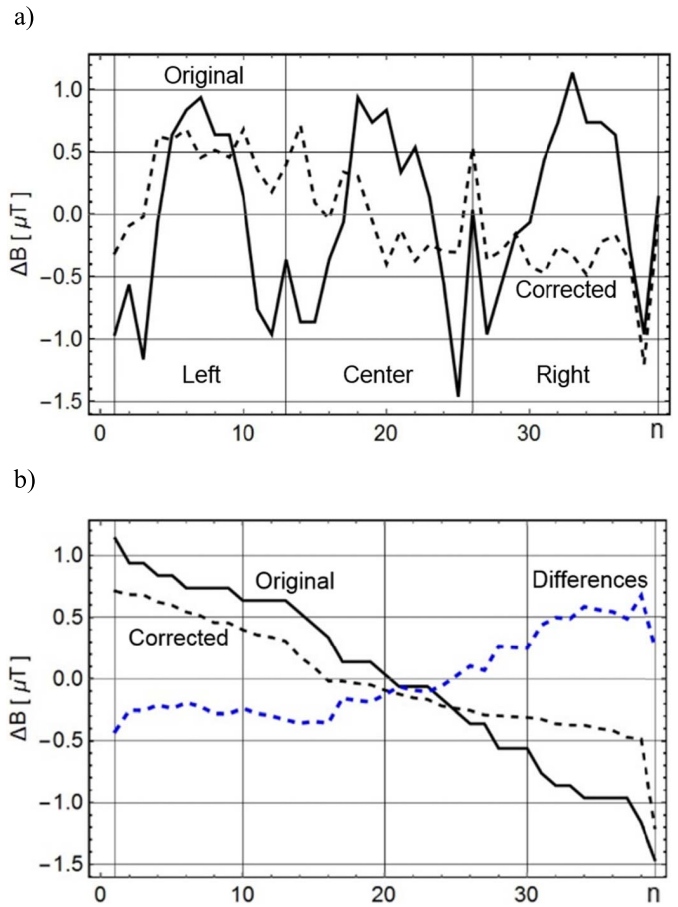


Fig. 7. (a) Graphical display of  $n = 39$  values of the magnetic field contributions (three planes in the  $z$ -direction, left, center, and right), measured by Bruker NMR Gaussmeter. (b) Values sorted according to size and differences.

- 5) List of contributions to the magnetic field in three planes in the  $z$ -direction, 39 values. The contributions are again measured in 39 points for each shim coil.
- 6) Writing of basic equations, calculation of the minimal and maximal values.
- 7) Calculation of shim currents using the algorithms of linear decomposition. Another possibility is a calculation utilizing a numeric optimization routine. Only small variation of the algorithm is necessary for such way of calculations.

In the next paragraphs, results of three methods of magnetic field measurements are graphically presented and resultant corrected magnetic field values interpreted in three planes and also sorted according to the size.

#### A. Hall Effect Measurement

For magnetic field measurements, the teslameter based on the Hall effect, type: MODEL 7010, (SYPRIS), precision:  $\pm 0.15 \mu\text{T}$  was used, it measured:  $x, y, z$  components. Measuring transducer was placed into the holes in the plastic holder (Fig. 4). Resultant values were in digital form. Measurement of magnetic field contributions from particular shim coils was performed without the basic magnetic field of the tomograph switched on. The resultant values were compared

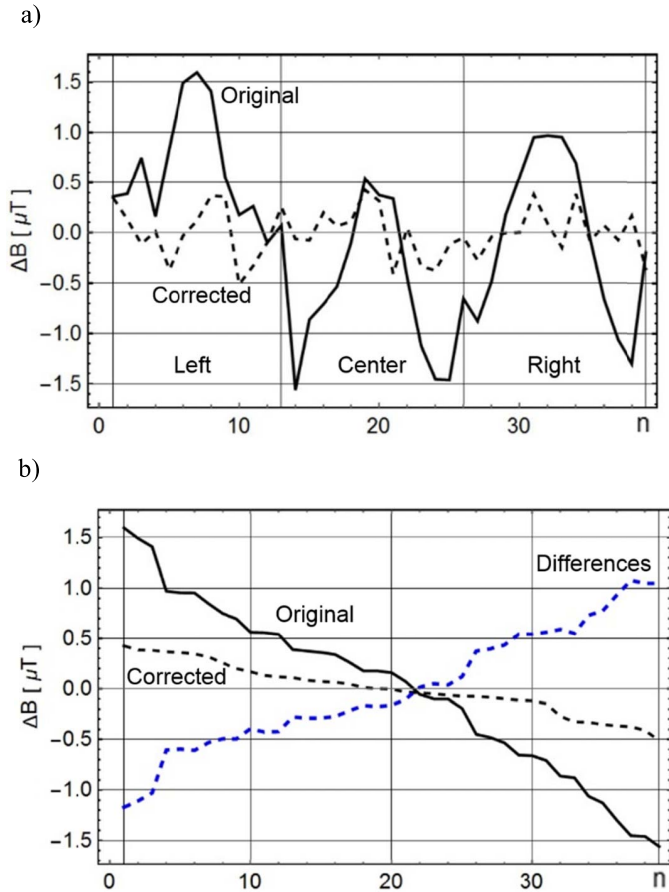


Fig. 8. (a) Graphical display of  $n = 39$  values of the magnetic field contributions (three planes in the  $z$ -direction, left, center, and right), measured by NMR method using GI imaging sequence. (b) Values sorted according to size and differences.

with magnetic field values measured in three parallel planes using NMR magnetometer.

**B. NMR Magnetometer Measurement**

For magnetic field measurements a magnetometer based on MR principles, Bruker NMR Gaussmeter ER035M, precision  $\pm 0.1 \mu T$  was used. Measurement was performed with basic magnetic field 0.1 T of the tomograph switched on.

Magnetometer based on MR principles measures the  $z$  component. Measuring transducer was placed into the holes in the plastic holder (Fig. 3). The “normal” value  $B_0 = B_z$  was measured in the center of the holder. In every measuring position of the circular modul, 13 magnetic field values were measured, switching 10 A current to the shim coils on and off.

**C. Imaging Measurement Method**

Magnetic field measurement method using GE imaging sequence of 13 capsules, cylindrical vessels, was applied (Fig. 4). Basic magnetic field 0.1 T of the tomograph was switched ON. In the imaging GE sequences, the following parameters were used:  $f_0 = 4.45$  MHz, samples per encoding: 256, phase encoding steps: 256, frequency bandwidth  $\pm 5000$  Hz,  $T = 100 \mu s$ , 24 accumulations, FOV =  $300 \times 300$  mm, slice thickness: 10 mm, TE = 33.7 ms,  $\Delta TE = 1$

TABLE I  
CALCULATED CURRENTS FOR PARTICULAR SHIM COILS IN [mA]

x	y	xy	yz	xz	$x^2-y^2$	$xz^2$
90.23	38.20	-29.11	39.64	149.61	32.41	14.56
$yz^2$	z	$z^2$	$z^2s$	$z^3$	$z^4$	$z^4s$
10.55	34.91	-160.96	170.96	-9.49	-111.41	-111.81



Fig. 9. Six-coil cylindrical resistive electromagnet 0.1 T.

ms, and TR = 300 ms. Measurement of  $z$  components was adjusted. Resultant values were proportional to the contrast levels of circular images calculated as average values of the imaging data.

**IV. IMAGING EXPERIMENT**

For experimental evaluation of the proposed method, a homemade resistive magnet 0.1 T, as a part of the whole-body imager, was used (Figs. 9 and 10):

- 1) diameter spherical volume: 400 mm;
- 2) the original inhomogeneity:  $\pm 1.5 \mu T$  (see Figs. 6–8).
- 3) mechanical adjustment: six-coil cylindrical resistive electromagnet, length 2055 mm, outer diameter 1414 mm, inner diameter 980 mm, and weight 5500 kg.

This resistive magnet in our laboratory allows testing several types of correcting systems and verifies several shim theories. Naturally, the designed shim methods are applicable on any MRI system with modifiable shim coils electronics.

Calculated shim currents using proposed imaging measurement method is depicted in Table I.

Fig. 11 shows images of a cylindrical homogeneous phantom, diameter 200 mm without and with magnetic field correction. Correcting currents were calculated using method C. For imaging, GE sequence was used, image size:  $256 \times 256$  pixels, slice thickness: 10 mm, and number of measurements: 2.

It is evident from Fig. 11 that quality of the picture with corrected magnetic field is significantly better (lower noise, higher homogeneity) in comparison with picture measured in non-corrected stationary magnetic field. Especially the phase image in non-corrected field shows  $8 \times 2\pi$  phase rotations, in corrected field, it is only  $4 \times 2\pi$  phase rotations.

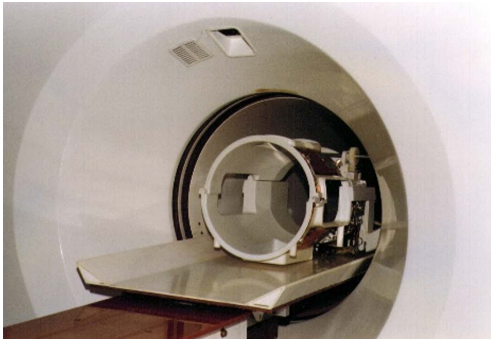


Fig. 10. Gantry of the whole-body 0.1 T NMR imager.

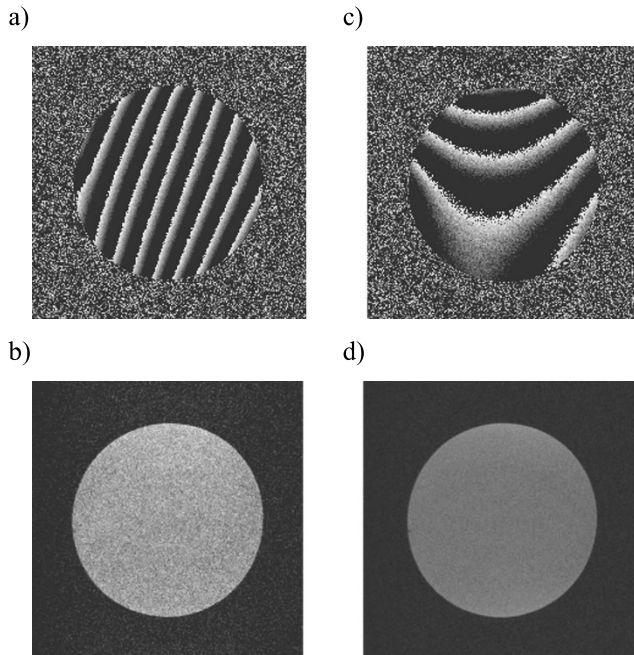


Fig. 11. MR images of a cylindrical phantom. (a) and (b) Phase and resultant images without corrections. (c) and (d) Phase and resultant images with shim corrections.

## V. CONCLUSION

The goal of this paper was comparative magnetic field measurements for homogeneity adjustment of MR imager.

Three measurement methods were used: the Hall effect, NMR magnetometer, and MR imaging. The experimental results were in good correlation with the mathematical simulations. Comparison of three methods showed little differences of measured results. The differences are given by different principles of measuring probes. Using the methods A and B, the results were read by an operator from an instant value (the output—last digit uncertainty, the operator estimated the average data). Using the method 3, the data are an average from a relative long-time operation (24 accumulations) without an influence of an operator.

The relative best results were achieved using the “imaging measurement method” (Fig. 8). The maximal differences were reduced. In the methods: “Hall effect” and “NMR magnetometer,” the maximal differences were  $\pm 1.0 \mu\text{T}$ , corrected values:  $\pm 0.5 \mu\text{T}$ . In the method: “Imaging measurement,” the maximal differences were  $\pm 1.5 \mu\text{T}$ , corrected values:  $\pm 0.4 \mu\text{T}$ .

Results of measurements and calculations provided concrete currents for shim coils adjustment. Measurements were performed on the whole-body resistive magnet 0.1 T. The final field homogeneity is given by superposition of the original field map and fields of calculated shimming coils currents. After adjusting the calculated shim currents to the correcting coils, the quality of MR images was significantly improved. The method is applicable for any higher number measuring of points, for any size of the cylinder, and for any higher number of measuring planes. This is an advantage of the described method.

It is evident that the “imaging measurement method” can be used only in the case of low inhomogeneities of the magnetic field, when it is possible to image all the capsules with acceptable signal to noise ratio. In the case of higher inhomogeneities, the methods using the Hall effect or NMR magnetometer must be used.

## ACKNOWLEDGMENT

This work was supported by the Scientific Grant Agency VEGA 2/0001/17, and within the project of the Research and Development Agency under Grant APVV-15-0029.

## REFERENCES

- [1] W. A. Anderson, “Electrical current shims for correcting magnetic fields,” *Rev. Sci. Instrum.*, vol. 32, no. 3, pp. 241–250 1961.
- [2] D. I. Hoult and D. Lee, “Shimming a superconducting nuclear-magnetic-resonance imaging magnet with steel,” *Rev. Sci. Instrum.*, vol. 56, no. 1, pp. 131–135 1985.
- [3] H. Siebold, “A computer program for optimizing homogeneous field magnets with iron yoke,” *IEEE Trans. Magn.*, vol. 24, no. 1, pp. 408–410, Jan. 1988.
- [4] P. Keller and P. Sommer, “Challenges in NMR magnetometry,” in *Proc. 21st IMEKO World Congr.*, vol. 1. Prague, Czech Republic, Aug./Sep. 2015, pp. 909–912.
- [5] P. Marcon, K. Bartusek, Z. Dokoupil, and E. Gescheidtova, “Diffusion MRI: Mitigation of magnetic field inhomogeneities,” *Meas. Sci. Rev.*, vol. 12, no. 5, pp. 205–212, 2012.
- [6] I. Frollo, P. Andris, I. Strolka, and L. Bačiak, “A least square method for measurement and optimisation in selected physical experiments,” *Key Eng. Mater.*, vols. 295–296, pp. 681–686, Oct. 2005.
- [7] C. J. Snape-Jenkinson, S. Crozier, and L. K. Forbes, “NMR shim coil design utilising a rapid spherical harmonic calculation method,” *ANZIAM J.*, vol. 43, no. 36, pp. 375–386, 2002.
- [8] R. Vadovic, “Aspects concerning the choice of measuring points and specification of parameters needed for a proper determination of magnetic fields,” *IEEE Trans. Magn.*, vol. 28, no. 3, pp. 1826–1832, May 1992.
- [9] T. Tadic and B. G. Fallone, “Design and optimization of a novel bored biplanar permanent-magnet assembly for hybrid magnetic resonance imaging systems,” *IEEE Trans. Magn.*, vol. 46, no. 12, pp. 4052–4058, Dec. 2010.
- [10] T. Tadic and B. G. Fallone, “Three-dimensional nonaxisymmetric pole piece shape optimization for biplanar permanent-magnet MRI systems,” *IEEE Trans. Magn.*, vol. 47, no. 1, pp. 231–238, Jan. 2011.
- [11] R. Vadovic, “Magnetic field correction using magnetized shims,” *IEEE Trans. Magn.*, vol. 25, no. 4, pp. 3133–3139, Jul. 1989.
- [12] Z. He, W. He, and J. Guo, “An optimized passive shimming method for bi-planar permanent MRI magnets,” *Appl. Magn. Res.*, vol. 48, no. 9, pp. 871–887, 2017.
- [13] H. S. Lopez, F. Liu, E. Weber, and S. Crozier, “Passive shim design and a shimming approach for biplanar permanent magnetic resonance imaging magnets,” *IEEE Trans. Magn.*, vol. 44, no. 3, pp. 394–402, Mar. 2008.
- [14] L. K. Forbes and S. Crozier, “Asymmetric zonal shim coils for magnetic resonance applications,” *Med. Phys.*, vol. 28, no. 8, pp. 1644–1651 2001.

- [15] L. K. Forbes and S. Crozier, "A novel target-field method for finite-length magnetic resonance shim coils: I. Zonal shims," *J. Phys. D, Appl. Phys.*, vol. 34, no. 24, pp. 3447–3455, 2001.
- [16] L. K. Forbes and S. Crozier, "A novel target-field method for finite-length magnetic resonance shim coils: II. Tesseral shims," *J. Phys. D, Appl. Phys.*, vol. 35, no. 9, pp. 839–849, 2002.
- [17] L. K. Forbes and S. Crozier, "A novel target-field method for magnetic resonance shim coils: III. Shielded zonal and tesseral coils," *J. Phys. D, Appl. Phys.*, vol. 36, no. 2, pp. 68–80, 2003.
- [18] S. Crozier, L. K. Forbes, and M. Brideson, "Ellipsoidal harmonic (Lame) MRI shims," *IEEE Trans. Appl. Supercond.*, vol. 12, no. 4, pp. 1880–1885, Dec. 2002.
- [19] M. A. Brideson, L. K. Forbes, and S. Crozier, "Winding patterns for actively shielded shim coils with asymmetric target-fields," *Meas. Sc. Techn.*, vol. 14, no. 4, pp. 484–493, 2003.
- [20] Z. Ni, Q. Wang, and C. Wang, "Design of axial shim coils for magnetic resonance imaging," *IEEE Trans. Appl. Supercond.*, vol. 21, no. 3, pp. 2084–2087, Jun. 2011.
- [21] H. Yang, W. Qiu-Liang, L. Yi, Z. Xu-Chen, and N. Chao-Qun, "Optimization of magnetic resonance imaging high-order axial shim coils using boundary element method," *Acta Phys. Sinica*, vol. 65, no. 21, p. 218301, 2016.
- [22] S. Kan, Q. Bao, F. Chen, C. Huang, J. Feng, and C. Liu, "Gradient shimming based on regularized estimation for  $B_0$ -field and shim functions," *J. Magn. Reson.*, vol. 268, pp. 1–9, Jul. 2016.
- [23] Y. Hu, X. Hu, L. Yan, Y. Fang, and W. Chen, "Shim coil set for an open biplanar MRI system using an inverse boundary element method," *IEEE Trans. Appl. Supercond.*, vol. 27, no. 7, Jul. 2016, Art. no. 4403905.
- [24] A. Mitsushi, "Passive shimming of MRI static magnetic field using regularization of truncated singular value decomposition," *Magn. Reson. Med. Sci.*, vol. 16, no. 4, pp. 284–296, 2017.
- [25] H.-H. Chen, R. D. Boykin, G. D. Clarke, J.-H. T. Gao, and J. W. Roby, "Routine testing of magnetic field homogeneity on clinical MRI systems," *Med. Phys.*, vol. 33, no. 11, pp. 4299–4306, 2006.
- [26] C. Z. Cooley *et al.*, "Two-dimensional imaging in a lightweight portable MRI scanner without gradient coils," *Magn. Reson. Med.*, vol. 73, no. 2, pp. 872–883, 2015.
- [27] P. J. Reber, Eric . C. Wong, R. B. Buxton, and L. R. Frank, "Correction of off resonance-related distortion in echo-planar imaging using EPI-based field maps," *Magn. Reson. Med.*, vol. 39, no. 2, pp. 328–330, 1998.
- [28] C. Windischberger, S. Robinson, A. Rauscher, M. Barth, and E. Moser, "Robust field map generation using a triple-echo acquisition," *J. Magn. Reson. Imag.*, vol. 20, no. 4, pp. 730–734, 2004.